

## N O T I C E

THIS DOCUMENT HAS BEEN REPRODUCED FROM  
MICROFICHE. ALTHOUGH IT IS RECOGNIZED THAT  
CERTAIN PORTIONS ARE ILLEGIBLE, IT IS BEING RELEASED  
IN THE INTEREST OF MAKING AVAILABLE AS MUCH  
INFORMATION AS POSSIBLE



# Technical Memorandum 80722

## The Helium Abundance of Jupiter From Voyager

(NASA-TM-80722) THE HELIUM ABUNDANCE OF  
JUPITER FROM VOYAGER (NASA) 37 P  
HC AC3/ME A01 CSCL 03B

N81-25015

Unclass  
63/91 25768

**D. Gautier, B. Conrath, M. Flasar, R. Hanel,  
V. Kunde, A. Chedin and N. Scott**

**OCTOBER 1980**

National Aeronautics and  
Space Administration

**Goddard Space Flight Center**  
Greenbelt, Maryland 20771



THE HELIUM ABUNDANCE OF JUPITER FROM  
VOYAGER

By

D. Gautier  
Observatoire de Paris  
9190 Meudon, France

B. Conrath, M. Flasar, R. Hanel, V. Kunde  
Laboratory for Extraterrestrial Physics  
NASA/Goddard Space Flight Center  
Greenbelt, Maryland 20771

A. Chedin, N. Scott  
Laboratoire de Meteorologie Dynamique  
Palaiseau, France

May 1980  
Revised October 1980

Submitted for Publication in  
Journal of Geophysical Research

## Abstract

The helium abundance in the Jovian atmosphere is derived from Voyager 1 data by two methods. The first method uses only infrared spectra from selected locations on the planet while the second method uses a thermal profile independently derived from radio occultation measurements and infrared spectra recorded near the occultation point. A hydrogen mole fraction of  $0.897 \pm 0.030$  is obtained from the first method while the second method gives  $0.880 \pm 0.036$ , corresponding to helium mass fractions of  $0.19 \pm 0.05$  and  $0.21 \pm 0.06$  respectively. The estimated errors for the first method are primarily due to systematic uncertainties in the  $H_2$  and He absorption coefficients, while those for the second method result mainly from errors in the radio occultation profile and are less well known. Random errors in the measured infrared spectra are found to be negligible in both cases. The results are consistent with a uniform mix of hydrogen and helium within Jupiter's interior, but a modest amount of helium depletion ( $\Delta Y \leq 0.05$ ) cannot be excluded.

## Introduction

An accurate determination of the helium abundance in the atmosphere of Jupiter is of great importance to models of the planetary interior and of the solar system evolution. Jupiter's large planetary mass, combined with a low exospheric temperature, has prevented significant escape of hydrogen and helium since planetary formation, and the bulk composition of Jupiter should be similar to that of the primitive solar nebula. Therefore, a comparison of the atmospheric abundance of helium on Jupiter with estimates of solar and cosmic abundances may indicate whether helium differentiation has occurred within the planet.

Pressure induced absorption from  $H_2-H_2$  and  $H_2-He$  collisions accounts for a large fraction of the far infrared opacity of Jupiter (Trafton, 1967). Taking advantage of the different spectral dependences of the  $H_2-H_2$  and  $H_2-He$  absorption coefficients, Gautier and Grossman (1972) proposed a method of inferring the helium abundance from spectral measurements in the  $300-700\text{ cm}^{-1}$  region. This method has been used to estimate the hydrogen mole fraction for Jupiter from airborne-spectroscopic (Houck, et al., 1975; Gautier, et al., 1977) and Pioneer center-to-limb measurements (Orton and Ingersoll, 1976). However, the accuracy of the results was limited in the airborne measurements by the absolute calibration and lack of spatial resolution and in the Pioneer determination by the use of broad band filters and the implicit assumption of horizontal homogeneity in the temperature field. The Voyager IRIS data provide significant advantages over previous measurements. A large number of calibrated spectra were obtained from various locations on Jupiter with a spectral resolution of  $4.3\text{ cm}^{-1}$ . This permits the selection of data from locations where the effect of aerosols is expected to be small.

In a preliminary analysis of Voyager data, Hanel et al. (1979) estimated the helium mole fraction to lie between 0.08 and 0.14. In the present paper the estimate is refined through more extensive analyses following two different approaches. First, the inversion method of Gautier and Grossman (1972) is applied to the IRIS infrared spectra from clear areas; next, radio occultation profiles are combined with IRIS data acquired near the occultation

points. The sources of error associated with each approach are examined, and the implications of the results are discussed.

### Collision-Induced Absorption of H<sub>2</sub>

Both methods used in this investigation depend on calculations of synthetic Jovian spectra in the 280-600 cm<sup>-1</sup> region. Therefore, before proceeding to a discussion of the methods themselves, the formulation of collision induced H<sub>2</sub> absorption coefficients used in these calculations will be reviewed. The formulation is based on the recent laboratory and theoretical work of Birnbaum and Cohen (1976), Birnbaum (1978), and Cohen and Birnbaum (1980).

The H<sub>2</sub> absorption coefficients enter the radiative transfer equation through the expression for monochromatic optical depth,

$$\tau_{\nu} = \int [q^2 A + q(1-q) B] (P/P_{NTP})^2 (T_{NTP}/T)^2 dz,$$

where  $q$  is the mole fraction of H<sub>2</sub>,  $P$  is the total atmospheric pressure,  $T$  is the atmospheric temperature, and  $z$  is the geometric altitude. The hydrogen mole fraction is defined by

$$q = \frac{n_{H_2}}{n_{H_2} + n_{He} \dots}$$

where  $n$  is the number density of the corresponding gases. The collision-induced absorption coefficients for H<sub>2</sub>-H<sub>2</sub> and H<sub>2</sub>-He collisions are represented by  $A$  and  $B$ , respectively.

Molecular hydrogen has a center of symmetry and, consequently, no permanent dipole moment. However, a weak collision-induced dipole spectrum exists which creates significant absorption for the very long path lengths

encountered in the Jovian atmosphere; about 40 km atm are above the one bar level. The theory of collision-induced absorption in homonuclear molecules indicates the existence of an induced dipole which results from two distinct physical mechanisms. The first mechanism, quadrupole interaction, is relatively long range and anisotropic in nature. The second mechanism, electron overlap interaction, is relatively short range and has both isotropic and anisotropic terms. The major contribution to the absorption for H<sub>2</sub>-H<sub>2</sub> collisions is from the quadrupolar interaction, with a smaller contribution from anisotropic overlap. The isotropic overlap is forbidden by symmetry for H<sub>2</sub>-H<sub>2</sub> collisions, but for H<sub>2</sub>-He collisions it is the dominant factor. The quadrupolar and anisotropic overlap terms are approximately one tenth of the terms for H<sub>2</sub>-H<sub>2</sub> collisions because of the smaller polarizability of He.

The analytical collision-induced lineshape of Birnbaum and Cohen (1976) was used for A and B, along with the appropriate shape factors determined from laboratory data (Cohen and Birnbaum, 1980). The expression for A is

$$A \propto \nu I_Q^{11} \left[ \phi \Gamma(\nu, \tau_1^{11}, \tau_2^{11}) + \rho \Gamma(\nu - \nu_{02}, \tau_1^{11}, \tau_2^{11}) + \frac{\rho}{5} \rho_1 \Gamma(\nu - \nu_{13}, \tau_1^{11}, \tau_2^{11}) + \dots \right]$$

with  $\nu$  being the transition wavenumber,  $I_Q$  the summed intensity of the translational-rotational transitions due to contributions from the quadrupole and anisotropic overlap induced dipole,  $\rho$  a Boltzmann factor,  $\phi$  a sum over states,  $\Gamma$  a lineshape function, and  $\tau_1$  and  $\tau_2$  lineshape parameters controlling the width and shape of  $\Gamma$ . The 11 superscript is for H<sub>2</sub>-H<sub>2</sub> collisions. The first term in the brackets represents absorption in the translational modes, caused by a change in relative kinetic energy of two colliding H<sub>2</sub> molecules, while the remaining terms represent absorption in the rotational-translational modes by the resonance lines. All H<sub>2</sub> energy levels are assumed to be in local thermodynamic equilibrium.

The A absorption coefficient is illustrated in Fig. 1a and b for temperatures of 180 and 100 K, respectively. This range approximates the temperatures of atmospheric layers in which the H<sub>2</sub> lines are formed. The effect of temperature on the relative contribution from the translational mode (0-200 cm<sup>-1</sup>), the S(0) resonance line (354 cm<sup>-1</sup>) and the S(1) resonance line (587.7 cm<sup>-1</sup>) may be seen. At these low temperatures only the 2 lowest rotational states, J = 0 (para) and J = 1 (ortho), are significantly populated.

The B absorption coefficient for H<sub>2</sub>-He collisions is represented by

$$B \propto \nu \left[ I_q^{12} \left\{ \phi \Gamma(\nu, \tau_1^{12}, \tau_2^{12}) + \dots \right\} + I_o^{12} \Gamma(\nu, \tau_1^{12}, \tau_2^{12}) \right]$$

where the superscript 12 refers to H<sub>2</sub>-He collisions and the terms are as defined before. The second term in the rectangular bracket represents the absorption due to the isotropic overlap with I<sub>o</sub> being the overlap intensity.

The B absorption coefficient is also illustrated in Figs. 1a and b. The weaker absorption of the S lines, relative to A, is due to the weaker quadrupole induced dipole for He while the stronger translational band arises from the isotropic overlap term in B. This term leads to the enhancement of the H<sub>2</sub>-H<sub>2</sub> absorption coefficient which allows the helium abundance to be derived from the infrared spectrum.

The influence of He on the optical depth of H<sub>2</sub> in the Jovian atmosphere may be demonstrated by the ratio

$$R = \tau(q)/\tau(q') = 0.9$$

where the value q' = 0.9 is taken as representative of the true Jovian hydrogen mole fraction. This ratio is shown in Fig. 2 for a mean atmospheric temperature of 140 K, and for q = 1.0 and 0.8. For wavenumbers greater than  $\nu$

$300 \text{ cm}^{-1}$ ,  $R$  shows a strong dependence on  $q$ , but only a weak dependence on wavenumber. This behavior reflects the dominance of the  $\text{H}_2\text{-h}_2$  term in the expression for the optical depth. If the atmospheric temperature is known independently as a function of the total atmospheric pressure, the measured spectral radiance can be regarded as a function of  $q$  alone, and this strong sensitivity can then be exploited. This forms the basis of the combined IRIS-radio occultation method. The stronger wavenumber dependence of  $R$  in the  $200 \text{ cm}^{-1}$  region reflects the increased relative importance of the  $\text{H}_2\text{-He}$  term in the optical depth. This frequency dependent sensitivity to  $q$  forms the basis of the inversion method in which both the atmospheric temperature profile and  $q$  are retrieved from the spectral radiances alone. Unfortunately, the region of strongest wavenumber dependence is not accessible in the Jovian infrared spectrum because of interference from the rotational  $\text{NH}_3$  lines. In the accessible region  $280\text{-}600 \text{ cm}^{-1}$ , the wavenumber dependence is relatively small; however, with the large number and good quality of spectra obtained by the Voyager IRIS it is still possible to extract significant information as discussed in the following section.

### Inversion Method

The principle of the inversion method as applied to Jupiter can be understood from the following considerations. Within the  $S(0)$  and  $S(1)$  lines of the spectrum generally two or more wavenumbers exist for which the brightness temperatures are the same; see for example Fig. 8. Therefore, measurements at these wavenumbers must be redundant in the sense that unit optical depth occurs at approximately the same atmospheric pressure level, and the same portion of the temperature profile is sampled in each case. However, a small but detectable difference in the dependence of optical depth on  $q$  exists for each wavenumber as discussed in the preceding section. For this reason, the dependence on atmospheric temperature can be eliminated; only one value of  $q$  satisfies a given set of measurements at the redundant wavenumbers. In practice, temperature profiles are retrieved for various values of  $q$  from sets of radiances which include redundant points, for which the corresponding weighting functions are nearly coincident. The solution for  $q$  is then taken as that value for which the rms residual between measured and calculated

radiance is a minimum. The wavenumbers chosen for this analysis are 287, 310, 340, 365, 475, 530, and 602  $\text{cm}^{-1}$ .

Unrecognized sources of opacity such as clouds may cause errors. Since regions of strong 5  $\mu\text{m}$  emission are known to be relatively cloud free, only spectra with brightness temperatures greater than 250 K at 5  $\mu\text{m}$  were included in the analysis. On the basis of this criterion, 62 spectra were selected, the majority of which were from the North Equatorial Belt.

Each of the chosen spectra was inverted for various values of  $q$ , and the root mean square of the residuals was calculated as a function of  $q$ . A typical result is shown in Fig. 3 where the minimum occurs at  $q = 0.89$ , and a histogram of all minima of  $q$  for the 62 samples is given in Fig. 4. From this distribution we obtain a mean value of  $q = 0.897$  with a standard deviation  $\sigma = 0.015$  and a standard error of the mean  $\Delta q_M = 0.002$ . The small value of  $\Delta q_M$  indicates that the random errors due to the instrument noise have a negligible effect. However, systematic errors can be present due to calibration uncertainties and errors in the absorption coefficients.

The accuracy of the IRIS calibration depends on the stability of the instrument temperature (Hanel et al., 1981). During the time of the measurements the interferometer temperature was stable and the uncertainty in the instrument temperature was less than 0.1K. Such an effect is negligible for the retrieval of  $q$ .

According to Birnbaum (1978) errors in the  $\text{H}_2$  absorption coefficients probably do not exceed  $\pm 5\%$ . The most important effects for this work are attributable to systematic errors in the  $\text{H}_2\text{-H}_2$  and  $\text{H}_2\text{-He}$  components of the coefficients. Several possible forms of error have been examined. A frequency independent variation of both A and B of  $\pm 5\%$ , is found to result in an error  $\Delta q$  of  $\pm 0.005$ . The introduction of a frequency independent relative error in A or B alone produces a much stronger effect. Fig. 5 shows the error  $\Delta q$  as a function of the relative error  $\Delta B/B$ ; a similar diagram will result from  $\Delta A/A$ . Assuming upper limits for  $\Delta A/A$  and  $\Delta B/B$  of  $\pm 0.05$  we obtain an uncertainty for  $\Delta q$  of  $\pm 0.03$ .

Our final estimate of the hydrogen molar fraction from the inversion method is  $q = 0.897 \pm 0.030$ . As discussed, the uncertainty is primarily due to conservatively estimated systematic errors in the absorption coefficients, a factor often neglected by other authors.

### IRIS-Radio Occultation Method

The Voyager Radio Science team has derived temperature profiles from measurements acquired during occultation of the spacecraft by the Jovian atmosphere (Eshleman et al., 1979). The upper atmosphere temperatures obtained with this technique depend strongly on the boundary condition assumed at the top of the atmosphere, but below the tropopause the solutions become increasingly insensitive to the assumed boundary condition. Thirteen IRIS spectra were obtained in the vicinity of the Voyager 1 ingress occultation point ( $9^{\circ}$  to  $12^{\circ}$ S,  $59^{\circ}$  to  $67^{\circ}$ W) with a field of view of  $16^{\circ}$  in latitude and longitude projected on the planet. This area is considerably larger than the narrow channel the radio signals propagate through. The thermal profile retrieved from the infrared data by means of inversion techniques described by Conrath and Gautier (1980) is shown in Fig. 6. Also shown are temperature profiles derived from the radio occultation measurements (G. Lindal, private communication) for two different boundary conditions at the top of the atmosphere. The agreement between the occultation profiles and the IRIS profiles is good in the troposphere and acceptable in the stratosphere when the limited vertical resolution of the infrared measurements in this portion of the atmosphere is taken into consideration (Gautier and Revah, 1975; Hanel et al., 1977; Orton, 1977). The tropospheric agreement also suggests that the presence of clouds and haze did not have a strong effect on the profile derived from the infrared spectra.

The radio occultation profiles are derived under the assumption of a specific hydrogen mole fraction. Changing this value rescales the temperature and pressure at each level according to the relations

$$\frac{T}{4-2q} \approx \text{const.}$$

9

and

$$\frac{P}{4-2q} \approx \text{const.}$$

Warm occultation profiles derived for  $q = 0.94$  and  $0.06$  are shown in Fig. 7. This behavior provides a sensitive method for determination of the hydrogen to helium ratio. Radio occultation profiles are generated for several values of  $q$  and each profile is then used to calculate a corresponding spectrum which is compared to the measured spectrum. A value of  $q$  corresponding to the best fit is then selected. The calculated spectra are highly sensitive to the hydrogen mole fraction because a change in  $q$  results in changes in both the temperature profile and atmospheric transmission which act in the same sense. Only a weak dependence exists on the upper atmospheric boundary since the emission in the  $285\text{--}600\text{ cm}^{-1}$  spectral region originates predominantly in the troposphere.

Determinations of  $q$  have been made using both the ingress and egress profiles as given by Lindsay, et al. (1981). To demonstrate the sensitivity of the technique, results of calculations for the ingress profile are shown in Fig. 8 where the best fit is obtained for  $q = 0.875$ . Similar calculations for the egress profile were compared with an average of 14 IRIS spectra acquired near the egress point ( $0.7^{\circ}\text{N}$ ,  $313^{\circ}\text{W}$ ), and the best fit was obtained for  $q = 0.880$ .

The values of  $q$  obtained by this method are subject to several sources of error, including noise in the infrared spectra, calibration errors, inaccurate knowledge of absorption coefficients, and uncertainties in the occultation temperature profiles as well as possible interference from haze and clouds. Each of these sources will now be considered.

The noise equivalent spectral radiance (NESR) of Voyager 1 IRIS in the  $280\text{--}600\text{ cm}^{-1}$  spectral region does not exceed  $5 \cdot 10^{-9}$  watts  $\text{cm}^{-2}$   $\text{sr}^{-1}/\text{cm}^{-1}$  (Hanel et al., 1980) which results in a signal to noise ratio per spectrum of about 300 at  $285\text{ cm}^{-1}$  and 30 at  $600\text{ cm}^{-1}$ . These values correspond to errors in brightness temperatures of about  $0.15\text{K}$  at  $285\text{ cm}^{-1}$  and  $0.5\text{K}$  at  $600\text{ cm}^{-1}$ . An uncertainty of  $1\text{K}$  in the calculated or measured brightness temperature results in an error of about  $0.01$  in  $q$ ; therefore, if we make the conservative

assumption that the errors associated with an individual spectrum also apply to the 13 averaged spectra, an upper limit on the uncertainty in  $q$  due to the random noise is  $\Delta q = \pm 0.004$ .

During the measurement of the occultation points, the interferometer temperature was extremely stable, and accordingly the absolute calibration errors are estimated to be less than the random errors and have a negligible effect on the determination of  $q$ .

To estimate the effect of absorption coefficient errors, outgoing spectra have been calculated with the total absorption coefficient modified by  $\pm 5\%$ . The results in terms of brightness temperature are shown in Fig. 9. The amplitude of the effect depends on the lapse rate in the atmospheric region where the emission originates. The effect is weak at  $600 \text{ cm}^{-1}$ , which corresponds to the tropopause level and is a maximum at  $270 \text{ cm}^{-1}$  which corresponds to the beginning of the convective zone. These brightness temperature changes imply that absorption coefficient errors result in an uncertainty in  $q$  of about  $\Delta q = \pm 0.005$ .

The effect of hazes and clouds may be noticeable at spectral intervals in which the emission emerges from deep atmospheric layers, such as the  $450\text{--}500 \text{ cm}^{-1}$  range and below  $300 \text{ cm}^{-1}$ . This may account for the residual differences over these intervals between calculated and measured spectra in Fig. 8. However neither haze nor clouds are expected to significantly affect the broad centers of the S(0) and S(1) lines near  $350$  and  $600 \text{ cm}^{-1}$ . Therefore the match between measured and calculated spectra was optimized for the spectral regions near the line centers. Thus, the errors due to unrecognized haze and cloud effects are expected to be small. However, no quantitative estimate has been made.

The principal uncertainty in the determination of  $q$  comes from the uncertainty in the occultation profiles. Lindal, et al. (1981) indicate that the tropospheric portion of the ingress profile is less reliable than the egress profile because of the presence of strong turbulence below the 300 mbar level at the ingress occultation point. For this reason only the egress

profile will be considered further in the present analysis. Estimation of the uncertainties in the egress profile is difficult since a detailed error analysis has not been published. Lindal et al. quote an error of  $\pm 7\text{K}$  at 1000 mbar and indicate the main error source is uncertainty in  $q$ . For purposes of this analysis we shall assume that in the absence of an uncertainty in  $q$ , the error in temperature would be  $\pm 3.5\text{K}$  which is half of the quoted total error.

This value is also consistent with an error estimate of 5 to 10K at the  $3\sigma$  level given previously by Eshelman, et al. (1979). An error of  $\pm 3.5\text{K}$  in the occultation profile results in an uncertainty of  $\pm 0.035$  in the inferred value of  $q$ .

If the various uncertainties discussed above are treated as statistically independent sources of error, then the final result obtained with this method is  $q = 0.880 \pm 0.036$ .

### Discussion and Conclusions

The hydrogen mole fraction for the atmosphere of Jupiter in the region between approximately 200 and 500 mb has been derived from Voyager data using two approaches. The inversion method applied to IRIS data from clear belt regions yields

$$q = 0.897 \pm 0.030$$

while the combined IRIS-radio occultation method gives

$$q = 0.880 \pm 0.036.$$

Fig. 10 and Table 1 compare the helium abundance derived in the present work with those determined from previous infrared observations of Jupiter's atmosphere by aircraft (Houck et al. 1975; Gautier, et al., 1977) and by Pioneer 11 (Orton and Ingersoll, 1976). Abundances are expressed in terms of both  $q$  and the helium mass fraction. Neglecting the small effect of heavy elements, the helium mass fraction is approximately

$$y \approx \frac{1-q}{1-0.5q}.$$

Because of the present uncertainty in the error estimate for the IRIS-radio occultation method, we have chosen to use the value derived from the inversion method as a basis for comparison in Fig. 10. Within the quoted errors, the Voyager IRIS determination agrees with those of the previous infrared investigations. The improvement afforded by the present study is actually greater than depicted in Fig. 10, since the errors quoted in the earlier works omitted estimates of systematic errors, especially those arising from inaccurate absorption coefficients.

The present atmospheric helium abundance of Jupiter may differ from the planet's bulk composition, because of helium differentiation during the planets's evolution. Differentiation is possible either because helium and hydrogen are immiscible over a range of temperatures and pressures relevant to Jupiter's interior, or because the metallic-molecular hydrogen transition near 3 Mbars is first-order, implying a discontinuity in helium abundance across the phase boundary. Experiments performed by Streett (1973) on hydrogen-helium fluid mixtures at pressures up to 9.3 kbars and temperatures from 26 to 100K have indicated the existence of separated fluid phases. Stevenson and Salpeter (1977a, b) have theoretically studied the phase behavior of hydrogen-helium fluids at the higher temperatures and pressures characteristic of Jupiter's interior and have considered the possible conditions for helium differentiation. They conclude that the present atmospheric abundance of helium can range from values which are consistent with the primordial mix to values significantly less. The uncertainty in the relevant thermodynamics makes it difficult to predict when in the evolution of the planet differentiation would begin.

Considerations based on energetics, however, can place constraints on the amount of helium differentiation which has occurred within the planet. That Jupiter radiates more energy than it absorbs from the Sun is well established (see Hanel et al. (1981) and references therein). Two major sources can account for this luminosity excess (Flasar, 1973; Salpeter, 1973): first,

cooling of the thermal reservoir produced by gravitational energy during an earlier quasi-gaseous contraction phase of Jupiter, and second, gravitational separation of hydrogen from helium during the current epoch. Homogeneous evolutionary models of Jupiter, which do not include helium differentiation, predict that the internal luminosity of Jupiter decays to its currently observed value in 4.5 billion years, the approximate age of the solar system (Graboske et al., 1975; Pollack et al., 1977; Hubbard, 1977; Grossman et al., 1980). Significant helium differentiation would increase the decay time by a factor of 5 (Stevenson and Salpeter, 1977b). Homogeneous evolutionary models of Saturn, on the other hand, predict luminosity decay times of only 2 billion years (Pollack et al., 1977; Grossman et al., 1980). These results suggest that helium differentiation has not, or has only recently, begun on Jupiter, but that significant differentiation has already occurred within Saturn. The atmospheric helium abundance of Jupiter would then be close to its primordial value; Saturn's would be depleted. Grossman et al. (1980) have estimated that the depletion on Jupiter, would be less than  $\Delta Y = 0.04$ ; Stevenson (1980) has estimated that the depletion in Saturn's atmosphere may amount to  $\Delta Y \approx 0.1$ .

Whether Jupiter's atmosphere is depleted in helium can, in principle, be independently determined by a comparison with cosmic and solar abundances. The present helium content of the universe is composed of a primordial component, produced in the big bang and the helium subsequently produced in stars. The observed large-scale homogeneity and isotropy of the universe suggest that the primordial component is distributed uniformly. The stellar component is distributed nonuniformly because the amount of stellar nucleosynthesis has varied from place to place. Since nucleosynthesis results in a net increase in helium, a primordial cosmic helium abundance greater than that presently measured in Jupiter's atmosphere would provide indirect evidence for differentiation. Greenstein (1980) has reviewed the various techniques used to infer the primordial cosmic helium abundance; systematic errors in these methods are difficult to assess. One approach is to determine the helium content of very old stars. Carney has applied stellar evolution calculations to population II subdwarfs and concludes  $Y = 0.19 \pm .04$ . Carney's result, however, is sensitive to the assumed abundance ratio O/Fe and to the parallax data used to infer the distances of the subdwarfs.

Probably the most reliable determination of the primordial helium abundance has come from emission line measurements of predominantly extragalactic objects. To determine the primordial helium abundance, Lequeux et al. (1979) observed blue compact galaxies and HII regions within irregular galaxies, and used earlier measurements of Orion and of the Large and Small Magellanic Clouds; French (1980) observed Markarian and Zwicky compact galaxies which are spectroscopically similar to HII regions; Talent (1980) observed HII regions within irregular and late-type spiral galaxies. The measurements have furnished helium abundances as a function of heavy element abundance. Extrapolating the heavy element abundance to zero provides an estimate of the primordial helium abundance. Considering the different objects observed, it is rather remarkable that the three determinations agree so well (cf. Table 1 and Fig. 10):  $Y_p \approx 0.22-0.23$  with an uncertainty of less than 0.02. Within the quoted errors, these abundances are consistent with the current determination for Jupiter's atmosphere (Fig. 10).

A more direct way of determining whether Jupiter's atmosphere is depleted in helium is to examine the helium abundance of the Sun, since both bodies presumably condensed from the same gas cloud. Observations of helium emission lines in the chromosphere and in prominences, and measurements of the relative abundances of cosmic rays both yield  $Y \approx 0.21$  with a typical error of approximately 0.04 (cf. Table 1 and Fig. 10). The question arises as to how representative these values are of the solar composition. The traditional view, from stellar structure calculations, is that the core of the Sun is radiative and is surrounded by a thermally convective envelope. No exchange of material takes place between the solar atmosphere and the central region where nucleosynthesis occurs. The observable solar atmospheric composition therefore represents the initial helium abundance of the Sun, prior to nuclear burning, and is directly comparable to the Jovian helium abundance. There are grounds, however, for questioning the traditional view of internal mixing (see below); moreover, Hirshberg (1973) has stressed that large systematic errors can arise in the interpretation of the cosmic ray and helium emission line data, resulting in uncertainties far in excess of the quoted errors.

Stellar evolution models, fitting the mass, luminosity, and age of the Sun, offer another means of determining its helium abundance. "Standard"

models yield initial mass fractions  $Y_1 \approx .22-.24$  (Iben, 1969, Bahcall et al., 1973; Ulrich and Rood, 1973; Mazzitelli, 1979). A major difficulty with these models, however, is their inability to satisfactorily account for the anomalously low measured neutrino flux (Davis et al., 1971). Bahcall et al. (1973) have fit the low neutrino fluxes with models assuming a low heavy-element abundance, and find  $Y_1 = 0.115$ . Since, from the study of Stevenson and Salpeter (1977b), the present Jovian atmospheric helium abundance places a lower limit on the initial solar helium abundance, this low value is precluded by the current work (Fig. 10). If one breaks with the standard model and permits sufficiently rapid mixing throughout the solar interior, higher values of  $Y_1$  are consistent with the observed neutrino flux (Iben, 1969). Recently, Schatzmann et al. (1980) have argued that turbulent mixing within the radiative core of the Sun can be induced by the shear associated with differential rotation, and have parameterized this mixing in terms of a Prandtl mixing-length diffusion term. They are able to fit the age and luminosity of the Sun and the neutrino flux with  $Y_1 = 0.25$ . The degree of internal mixing within the Sun, however, is yet to be examined in a dynamically self-consistent fashion and remains an open issue.

The combined use of interior models with the measured spectrum of global oscillations on the surface of the Sun can also furnish an estimate of  $Y_1$ . Iben and Mahaffy (1973) obtained  $Y_1 = 0.19-0.21$  in this manner. More recently Isaak (1980), using new observations which resolved the broad 5 minute oscillation peak into several lines, concluded  $Y_1 < 0.17$ , but this limit appears to be inconsistent with the estimates of the primordial cosmic helium abundance discussed earlier. We conclude that a reliable estimate of the initial solar helium abundance remains elusive. The present determination for Jupiter may in fact represent the best estimate of the solar value to date.

To summarize, the estimated errors in the current determination of the helium composition in Jupiter's atmosphere, as well as uncertainties in both the solar and primordial cosmic abundance of helium, preclude a firm conclusion concerning helium differentiation within Jupiter. The results are consistent with a uniform mix of hydrogen and helium within Jupiter's interior, but a modest amount of depletion in the atmosphere ( $\Delta Y \leq 0.05$ ) cannot be excluded. Comparison with Saturn's helium abundance may prove to be

the most valuable diagnostic tool. An atmospheric helium abundance on Saturn lower than that on Jupiter would tend to support the arguments for differentiation based on energetics. A helium abundance comparable to that on Jupiter would alternatively open . possibility that significant differentiation has occurred on neither planet and therefore furnish an upper limit on the primordial cosmic helium abundance. The recent Pioneer 11 determination of Saturn's atmospheric helium abundance was not conclusive. The improved determination anticipated from Voyager IRIS is therefore essential for resolving this problem.

#### Acknowledgements

We are indebted to G. Lindal for providing radio occultation profiles prior to publication, and G. Orton for helpful discussions. We also thank R. Dufour for furnishing extracts of D. Talent's unpublished Ph.D. thesis and acknowledge J. Andouze, B. Carney, D. Kunth, H. French, J. Lequeux, E. Schatzman, M. Stite, F. Stecker, and S. and G. Vauclair for a series of enlightening conversations on the subject of astrophysical helium abundances.

## References

- Bahcall, J. N., W. F. Huebner, N. H. Magee, A. L. Mertz, and R. K. Ulrich, Solar neutrinos, IV. Effect of radiative opacities on calculative neutrino fluxes, Astrophys. J., 184, 1-4, 1973.
- Birnbaum, G., Far infrared absorption in H<sub>2</sub>-H<sub>2</sub> and H<sub>2</sub>-He mixtures, J. Quant. Spectrosc. Radiat. Transfer, 19, 51-62, 1978.
- Birnbaum, G. and E. R. Cohen, Theory of the line shape in pressure induced absorption, Canada J. Phys., 54, 593-602, 1976.
- Carney, B. W., The subdwarf helium abundance and the rotation of the galactic halo, Astrophys. J., 233, 877-887, 1979.
- Cohen, E.R., and G. Birnbaum, Analysis of the shape of the far infrared spectrum of H<sub>2</sub>, N.B.S.J. of Res., Submitted for publication, 1980.
- Conrath, B. J., and D. Gautier, Thermal structure of Jupiter's atmosphere obtained by inversion of Voyager 1 infrared measurements, in Interpretation of Remotely Sensed Data, A. Deepak, editor, Academic Press, New York, to be published, 1980.
- Davis, R. Jr., L. C. Rogers, and V. Radeka, Report on the Brookhaven solar neutrino experiment, Bull. Amer. Phys. Soc., 16, 631, 1971.
- Eshleman, V. R., G. L. Tyler, G. E. Wood, G. F. Lindal, J. D. Anderson, G. S. Levy, T. A. Croft, Radio science with Voyager 1 at Jupiter: Preliminary profiles of the atmosphere and ionosphere, Science, 204, 976-978, 1979.
- Flasar, F. M., Gravitational energy sources in Jupiter, Astrophys. J., 186, 1097-1106, 1973.
- French, H. B., Galaxies with the spectra of giant HII regions, Astrophys. J., 240, 15 Aug. 1980 issue.

- Gautier, D. and K. Grossman, A new method for the determination of the mixing ratio hydrogen to helium in the giant planets, J. Atmos. Sci., 29, 788-792, 1972.
- Gautier, D. and I. Revah, Sounding of the planetary atmospheres: A Fourier analysis of the radiative transfer equation, J. Atmos. Sci., 32, 881-892, 1975.
- Gautier, D., A. Lacombe and I. Revah, The thermal structure of Jupiter from infrared spectral measurements by means of a filtered iterative inversion method, J. Atmos. Sci., 34, 1130-1137, 1977.
- Graboske, H. C., Jr., J. B. Pollack, A.S. Grossman, and R. J. Olness, The structure and evolution of Jupiter: The fluid contraction stage, Astrophys. J., 199, 265-281, 1975.
- Greenstein, J. L., The evidence for a universal helium and deuterium abundance, Physica Scripta, 21, 759-768, 1980.
- Grossman, A. S., J. B. Pollack, R. T. Reynolds, A. L. Summers and H. G. Graboske, Jr., The effect of dense cores on the structure and evolution of Jupiter and Saturn. Icarus, 42, 358-379, 1980.
- Hanel, R., B. Conrath, D. Gautier, P. Gierasch, S. Kumar, V. Kunde, P. Lowman, W. Maguire, J. Pearl, J. Pirraglia, C. Ponnamperna, and R. Samuelson, The Voyager infrared spectroscopy and radiometry investigation, Space Science Reviews, 21, 129-157, 1977.
- Hanel, R., D. Crosby, L. Herath, D. Vanous, D. Collins, H. Creswick, C. Harris and M. Rhodes, Infrared spectrometer for Voyager, Applied Optics, 1391-1400, 1980.
- Hanel, R. A., B. J. Conrath, L. W. Herath, V. G. Kunde and J. A. Pirraglia, Albedo, internal heat, and energy balance of Jupiter; preliminary results of the Voyager infrared investigation, JGR, in press, 1981.

- Hirayama, T., The abundance of helium in prominences and in the chromosphere, Solar Phys., 19, 384-400, 1971.
- Hirsberg, J., Helium abundance of the Sun, Review of Geophysics and Space Physics, 11, 115-131, 1973.
- Houck, J. R., J. B. Pollack, D. Schack, R. A. Reed, and A. Summers, Jupiter: Its infrared spectrum from 16 to 40 micrometers, Science, 189, 720-722, 1975.
- Hubbard, W.B., The Jovian surface condition and cooling rate, Icarus, 30, 305-310, 1977.
- Iben, I., Jr., The  $\text{Cl}^{37}$  solar neutrino experiment and the solar helium abundance, Ann. Phys., 54, 164-203, 1969.
- Iben, I., Jr., and J. Mahaffy, On the Sun's acoustical spectrum, Astrophys. J. (Letters), 209, L39-L43, 1976.
- Isaak, G. R., Solar oscillations, stellar oscillations and cosmology, Nature, 283, 644-645, 1980.
- Kunth, D. and W. L. W. Sargent, private communication.
- Lambert, D. L., The Eleventh Herstmonceux Conference: helium, Observatory, 960, 199-200, 1967.
- Lequeux, J., M. Peimbert, J. F. Rayo, A. Serrano and S. Torres - Peimbert, Chemical composition and evolution of irregular and blue compact galaxies, Astron. Astrophys., 80, 155-166, 1979.
- Mazzitelli, I., Solar models, helium content and mixing length, Astron. Astrophys., 79, 251-253, 1979.

- Orton, G. S., Recovery of the mean Jovian temperature structure from inversion of spectrally resolved thermal radiance data, Icarus, 32, 41-57, 1977.
- Orton, G. S., and A. P. Ingersoll, Pioneer 10 and 11 and groundbased infrared data on Jupiter: The thermal structure and He-H<sub>2</sub> ratio, in Jupiter, edited by T. Gehrels, 207-215, University of Arizona press, Tucson, 1976.
- Orton, G. S., and A. P. Ingersoll, Saturn atmospheric temperature structure and heat budget, preprint of paper submitted to JGR, 1980.
- Pollack, J. B., A. S. Grossman, R. Moore, and H. C. Graboske, Jr., A calculation of Saturn's gravitational contraction history, Icarus, 30, 111-128, 1977.
- Salpeter, E. E., On convection and gravitational layering in Jupiter and in stars of low mass, Astrophys. J., 181, L89-92, 1973.
- Schatzman, E., A. Maeder, F. Angrand, and R. Glowinski, Stellar evolution with turbulent diffusion mixing, III. The solar model and the neutrino problem, Astron. Astrophys., submitted 1980.
- Stecker, F. W., Helium synthesis, neutrino flavors, and cosmological implications, Phys. Rev. Lett., 44, 1237-1240, 1980.
- Stevenson, D. J., Saturn's luminosity and magnetism, Science, 208, 746-747, 1980.
- Stevenson, D. J. and E. E. Salpeter, The phase diagram and transport properties for hydrogen-helium fluid planets, Astrophys. J. Suppl., 35, 221-237, 1977a.
- Stevenson, D. J., and E. E. Salpeter, The dynamics and helium distribution in hydrogen-helium fluid planets, Astrophys. J. Suppl., 35, 239-261, 1977b.

- Streett, W. B., Phase equilibria in molecular hydrogen-helium mixtures at high pressures, Astrophys. J., 186, 1107-1125, 1973.
- Talent, D. L., A spectrophotometric study of HII regions in chemically young galaxies, Ph.D. Thesis, Rice University, 1980.
- Trafton, L. M., Model atmospheres of the major planets, Astrophys. J., 147, 765-781, 1967.
- Ulrich, R. K., and R. T. Rood, Mixing in stellar models, Nature Phys. Sci., 241, 111-112, 1973.
- Yang, J., N. Schramm, G. Steigman, and R. T. Wood, Constraints on cosmology and neutrino physics from big bang nucleosynthesis, Astrophys. J., 227, 697-706, 1979.

Table 1. Summary of Helium Abundances

Determination	q	Y	Reference
<u>Jupiter</u>			
(a) Aircraft	.89 ± .11 .88+.12-.06	.20+.16-.20 .21+.09-.21	Houck, et al, 1975 Gautier, et al. 1977
(b) Pioneer 11	.88 ± .06	.21+.09-.10	Orton & Ingersoll, 1976
(c) Voyager IRIS (Inversion)	.897 ± .030	.19 ± .05	This investigation
(d) Voyager IRIS Radio Occultation (Egress)	.880 ± .036	.21 ± .06	This investigation
<u>Solar</u>			
(e) Helium Emission Lines	.88 ± .02	.21 ± .03	Mirayama, 1971
(f) Cosmic Rays		.20 ± .04	Lambert, et al. 1967
(g) Standard Interior Models (initial abundance)	.86 - .88	.22 - .24	Iben, 1969; Bahcall, et al., 1973; Ulrich & Rood, 1973; Mazzitelli, 1979; Yang, et al. 1979
(h) Low heavy element fit	.939	.115	Bahcall, et al. 1973
(i) Well mixed interior	.86	.25	Schatzmann, et al. 1980
(j) Solar oscillations	.88 - .90	.19 - .21	Iben and Mahaffy, 1976
(k) " "	>.91	<.17	Isaak, 1980
<u>Primordial</u>			
(l) Pop. II subdwarf	.90 ± .02	.19 ± .04	Carney, 1979
(m) Extragal. HII emission	.871 ± .009	.228 ± .014	Lequeux, et al. 1979
(n) " " "	.879 ± .009	.216 ± .015	French, 1980
(o) " " "	.879 ± .008	.216 ± .013	Talbot, 1980

## Figure Captions

Figure 1. Pressure-induced absorption coefficients for molecular hydrogen with hydrogen and with helium as the broadening gas. The upper part is for  $T = 100$  K and the lower for 180 K.

Figure 2. An illustration of the sensitivity of the optical depth in the Jovian atmosphere to the helium mole fraction.

Figure 3. Root mean square of the residuals between calculated and measured radiances as a function of the hydrogen mole fractions for one of the 62 spectra analyzed.

Figure 4. Histogram of the values of  $q$  retrieved from 62 IRIS spectra.

Figure 5. Estimate of the error in  $q$  resulting from a relative error  $\Delta B/B$  in the  $H_2$ -He component of the absorption coefficient.

Figure 6. "Warm"(W) and "cold"(C) thermal profiles derived from the radio occultation entry of Voyager 1, compared to a profile retrieved from an average of 13 infrared spectra recorded at approximately the same atmospheric location ( $12^\circ S$ ,  $63^\circ W$ ). The profiles are derived for a hydrogen mole fraction of 0.915. W and C are derived from boundary conditions of 155 K at 11.5 mb and of 145 K at 10.8 mb respectively.

Figure 7. Warm occultation profiles similar that of Figure 4, but derived for  $H_2$  mole fraction of 0.86 and 0.94.

Figure 8. Brightness temperature spectra calculated from the ingress occultation profile for  $q = 0.835$ ,  $q = 0.875$  and  $q = 0.915$ , compared to an average of 13 IRIS spectra measured near the location of the radio occultation entry.

Figure 9. Variations in brightness temperatures of the calculated spectrum resulting from variation of the total absorption coefficient by +5% and -5%.

Figure 10. Comparison of helium abundance determinations for Jupiter, the Sun, and selected astrophysical objects. The sources for the various values are: (a) Aircraft measurements (Houck et al., 1975; Gautier et al., 1977); (b) Pioneer 11 infrared radiometer (Orton and Ingersoll, 1976); (c) IRIS inversion method (this work); (d) IRIS-radio occultation method for the egress point (this work); (e) Solar chromospheric emission lines (Hirayama, 1971); (f) Cosmic rays (Lambert, 1967); (g) Standard evolution models (Iben, 1969; Bahcall et al., 1973; Ulrich and Rood, 1973; Mazetelli, 1979; Yang et al., 1979); (h) Low heavy-element model fit to neutrino flux (Bahcall et al., 1973); (i) Models with mixing throughout the interior (Schatzmann et al., 1980); (j) Iben and Mahaffy, 1976); (k) Isaak, 1980; (l) Carney, 1979; (m) Lequeux et al., 1979; (n) French, 1980; (o) Talent, 1980.

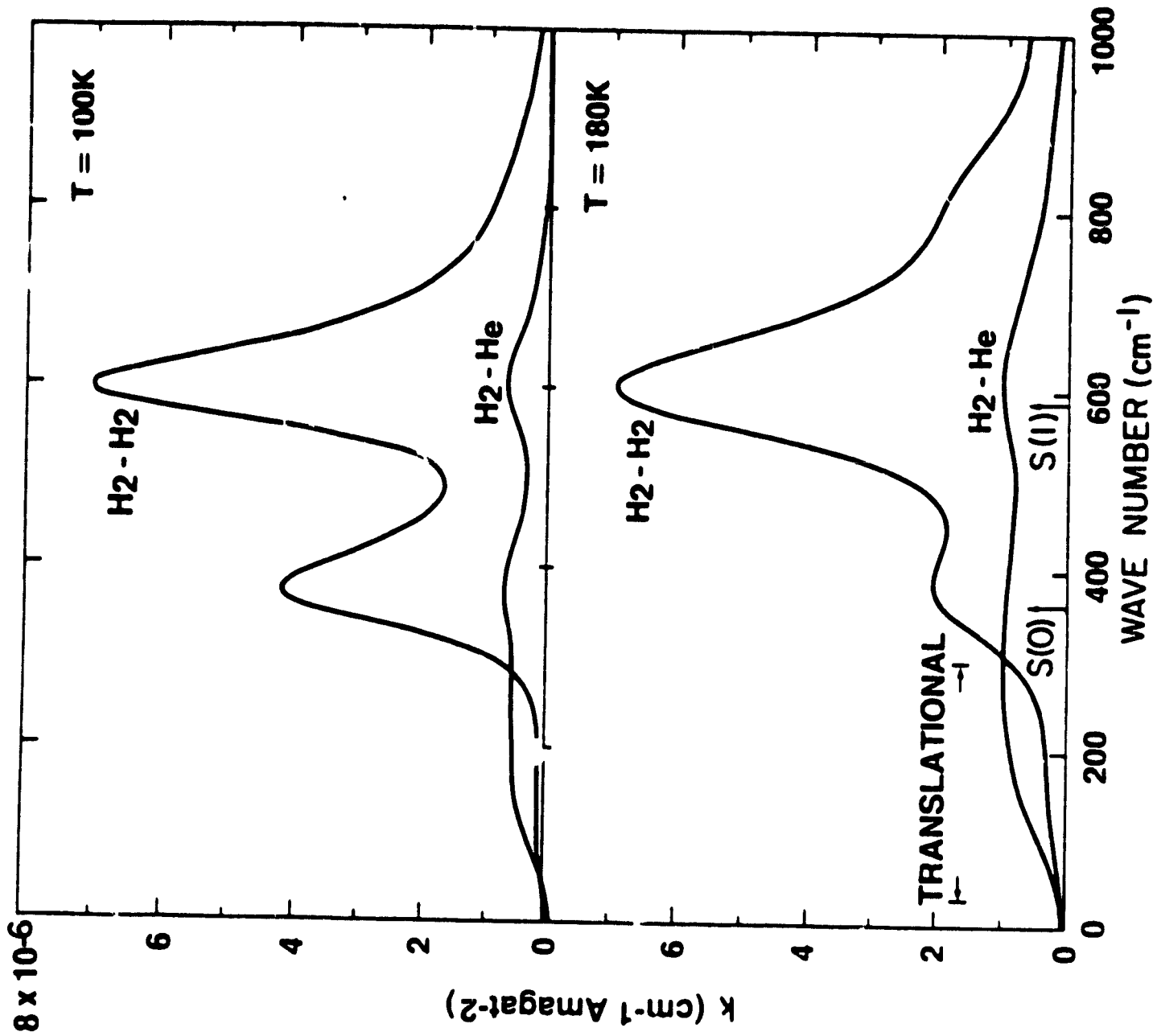


Figure 1

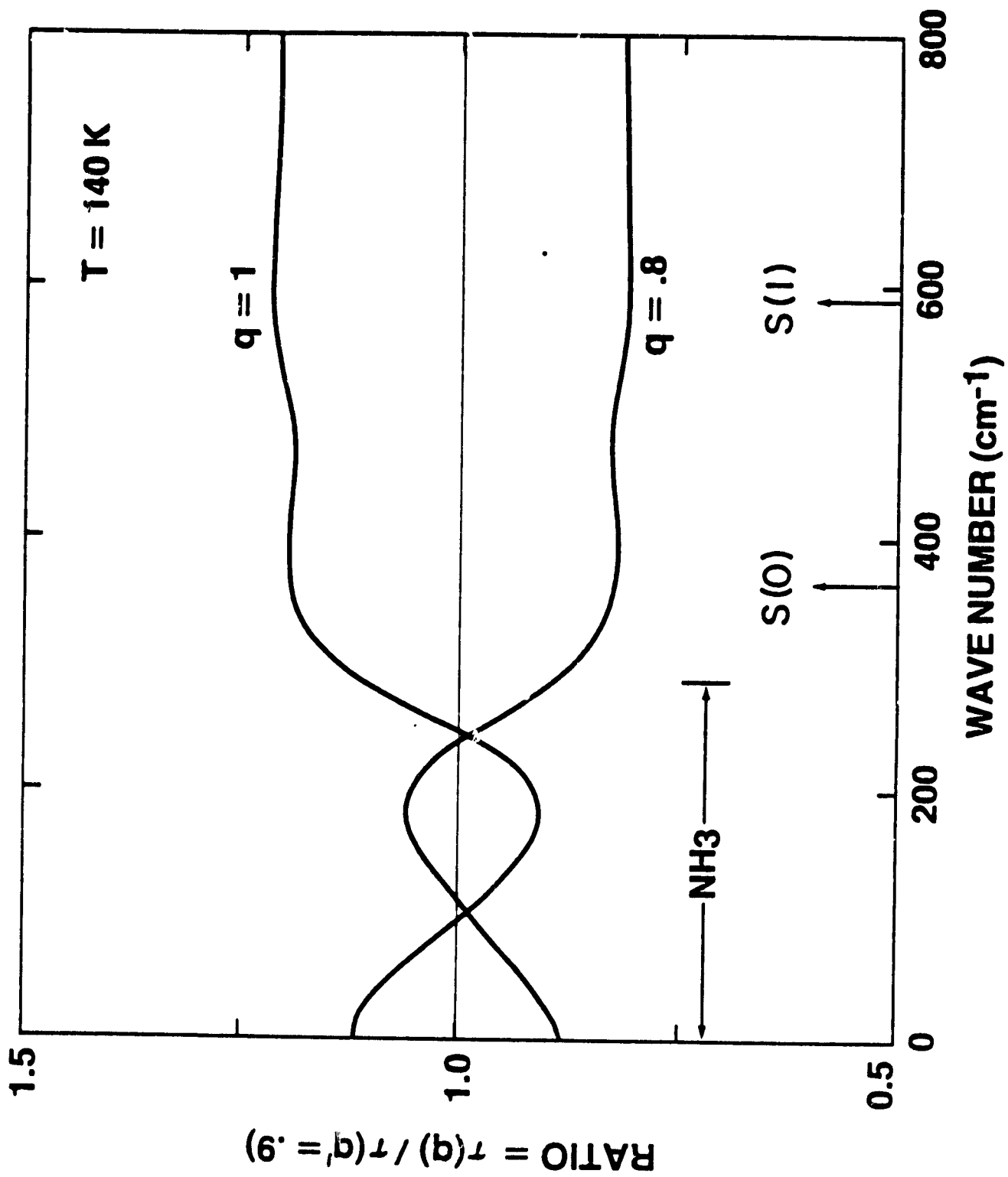


Figure 2

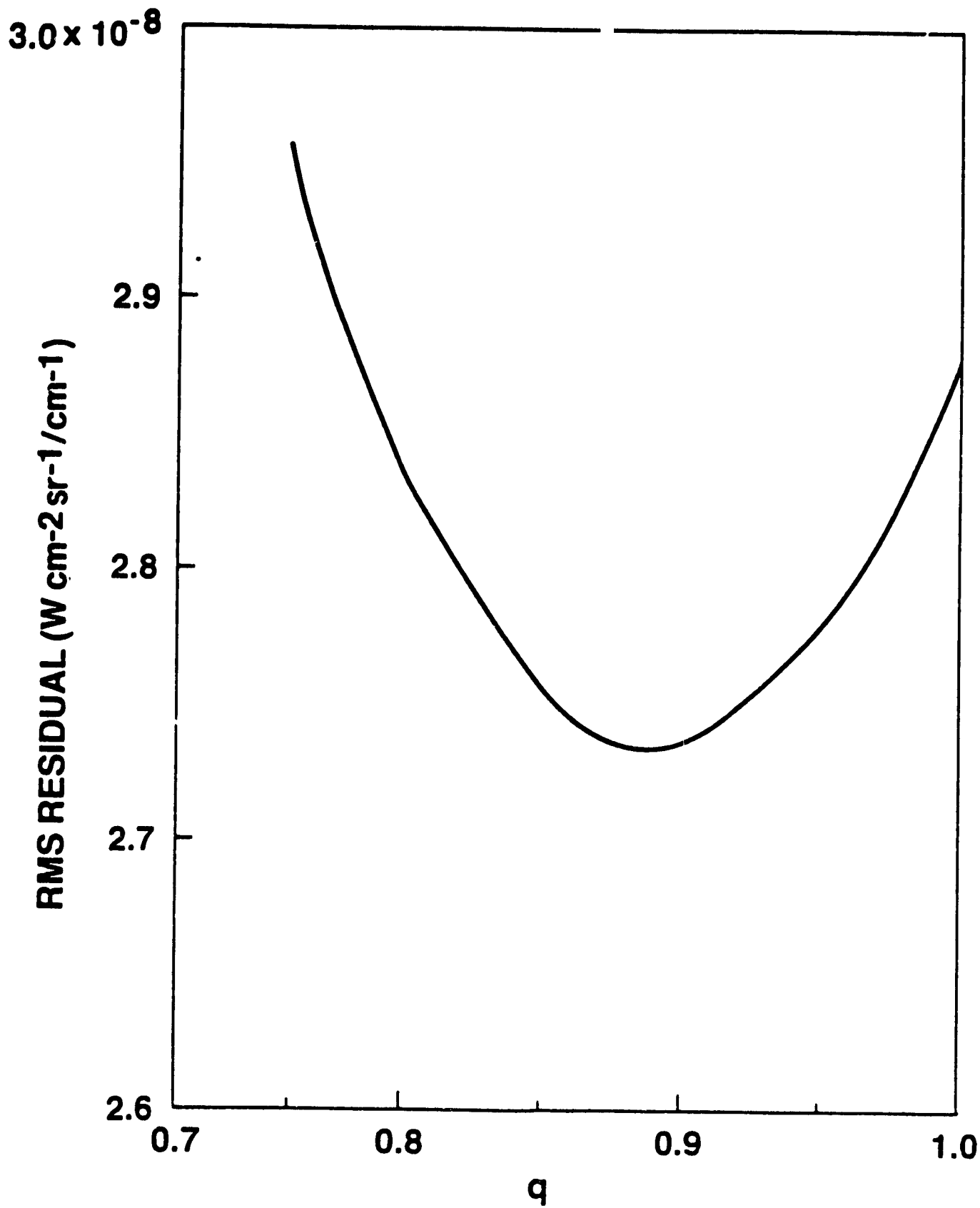


Figure 3

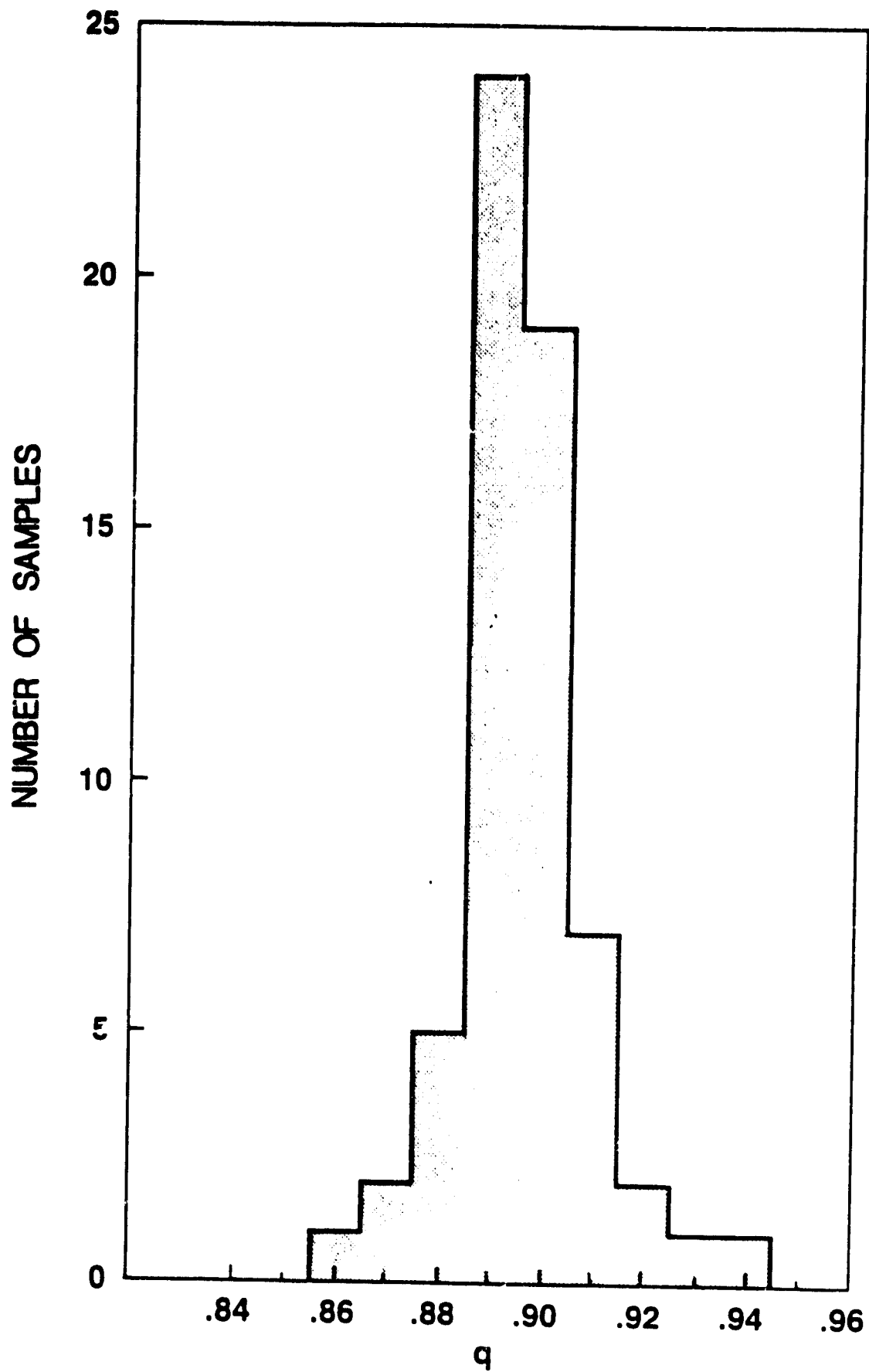


Figure 4

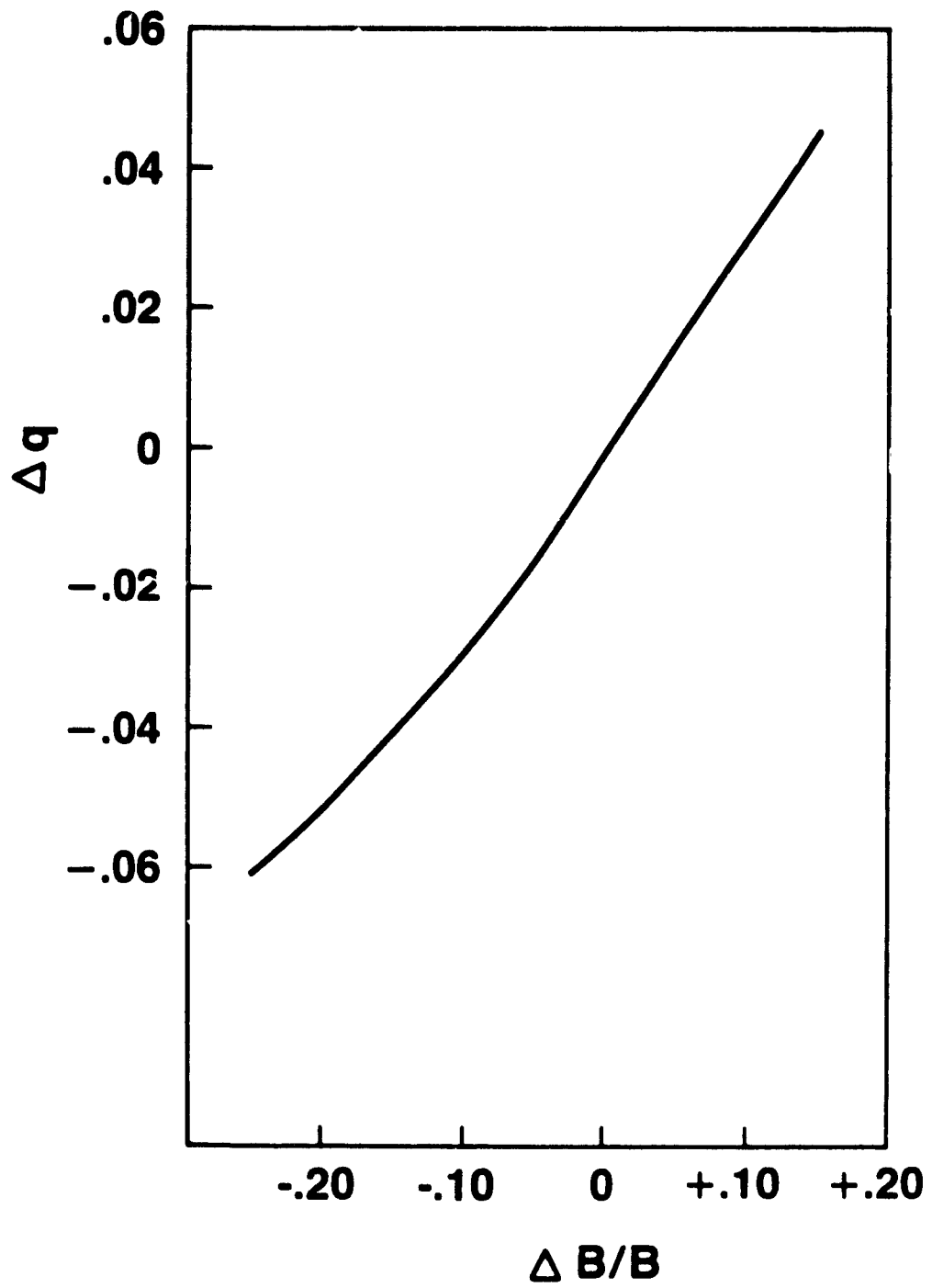


Figure 5

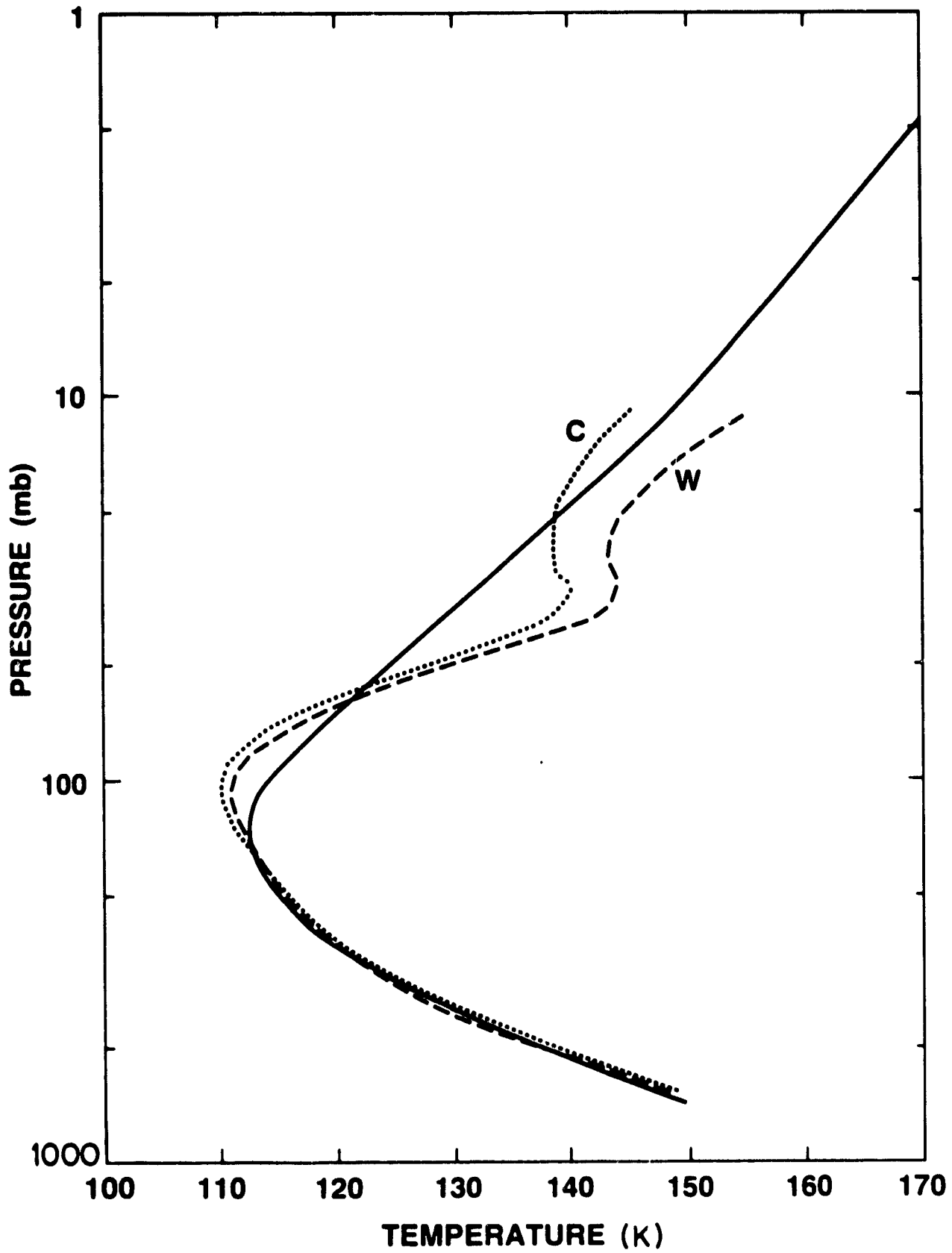


Figure 6

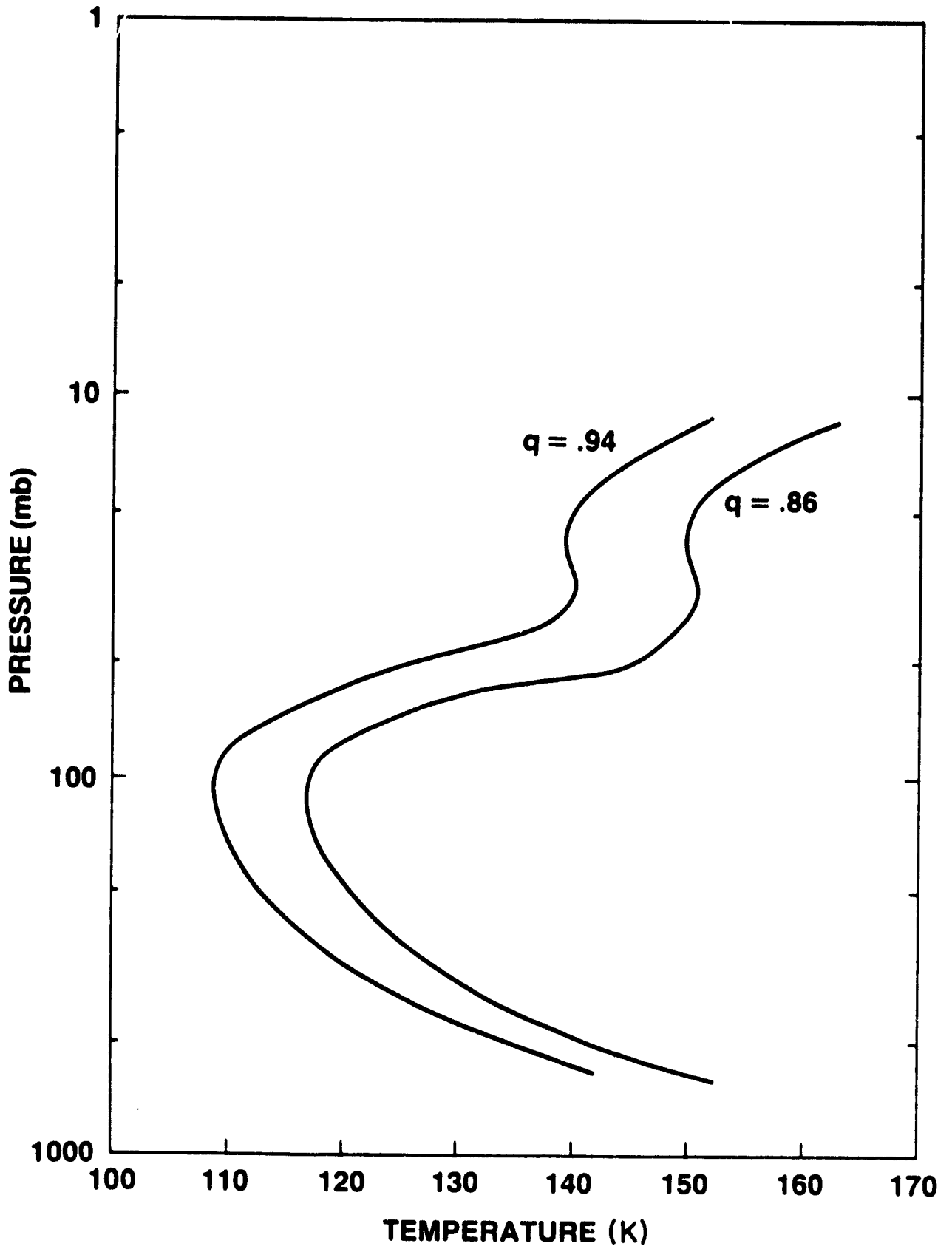


Figure 7

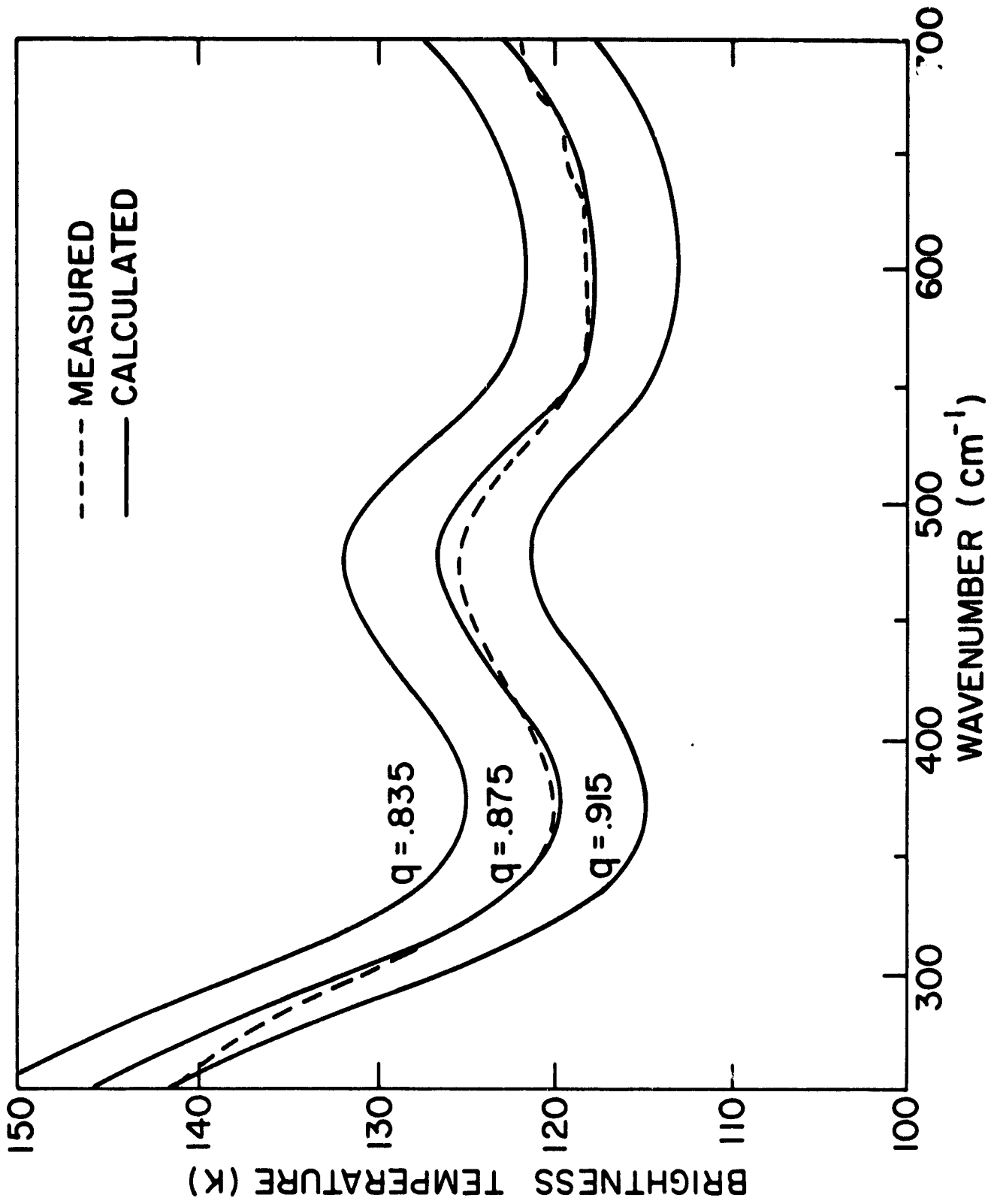


Figure 8

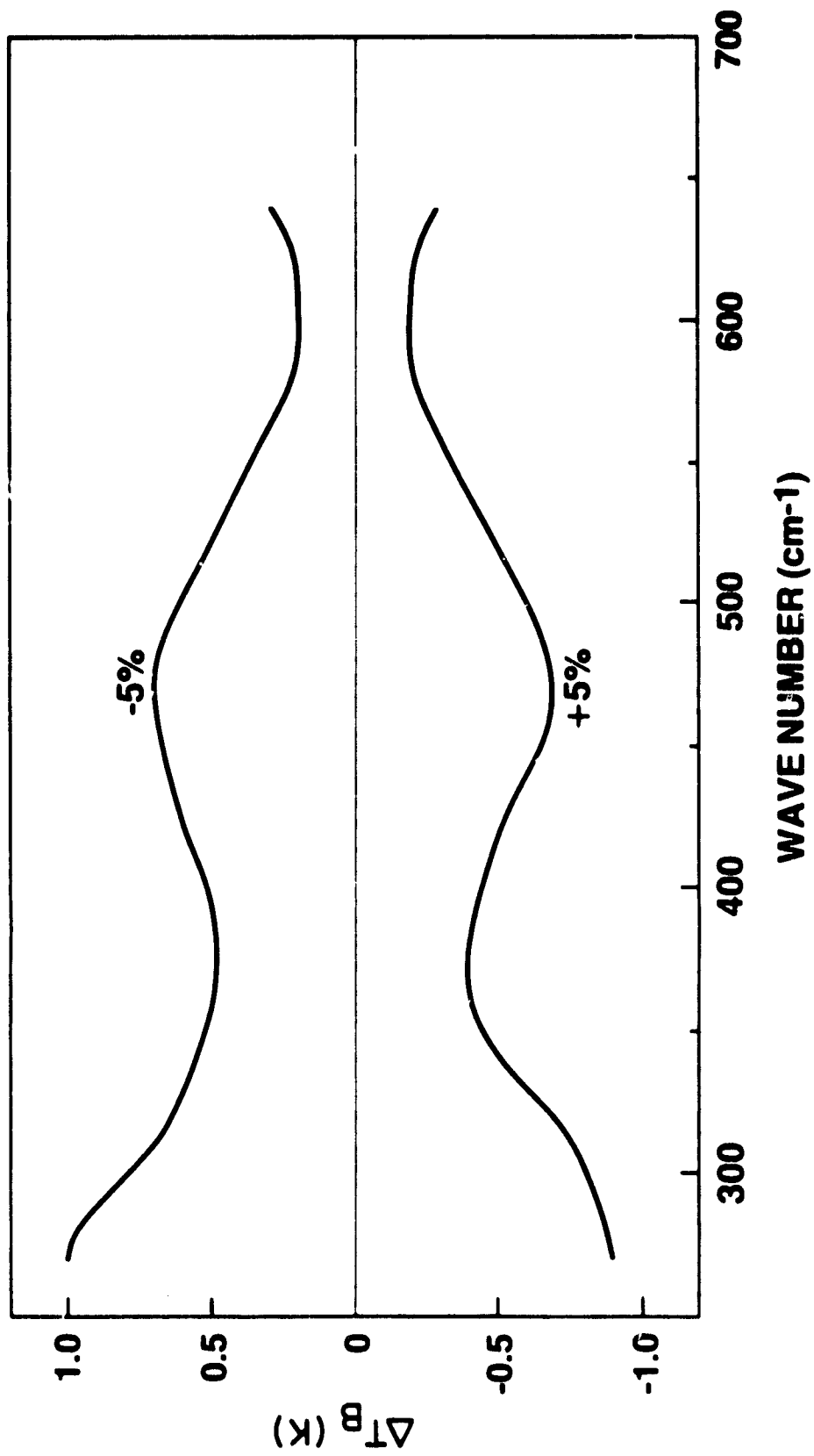


Figure 9

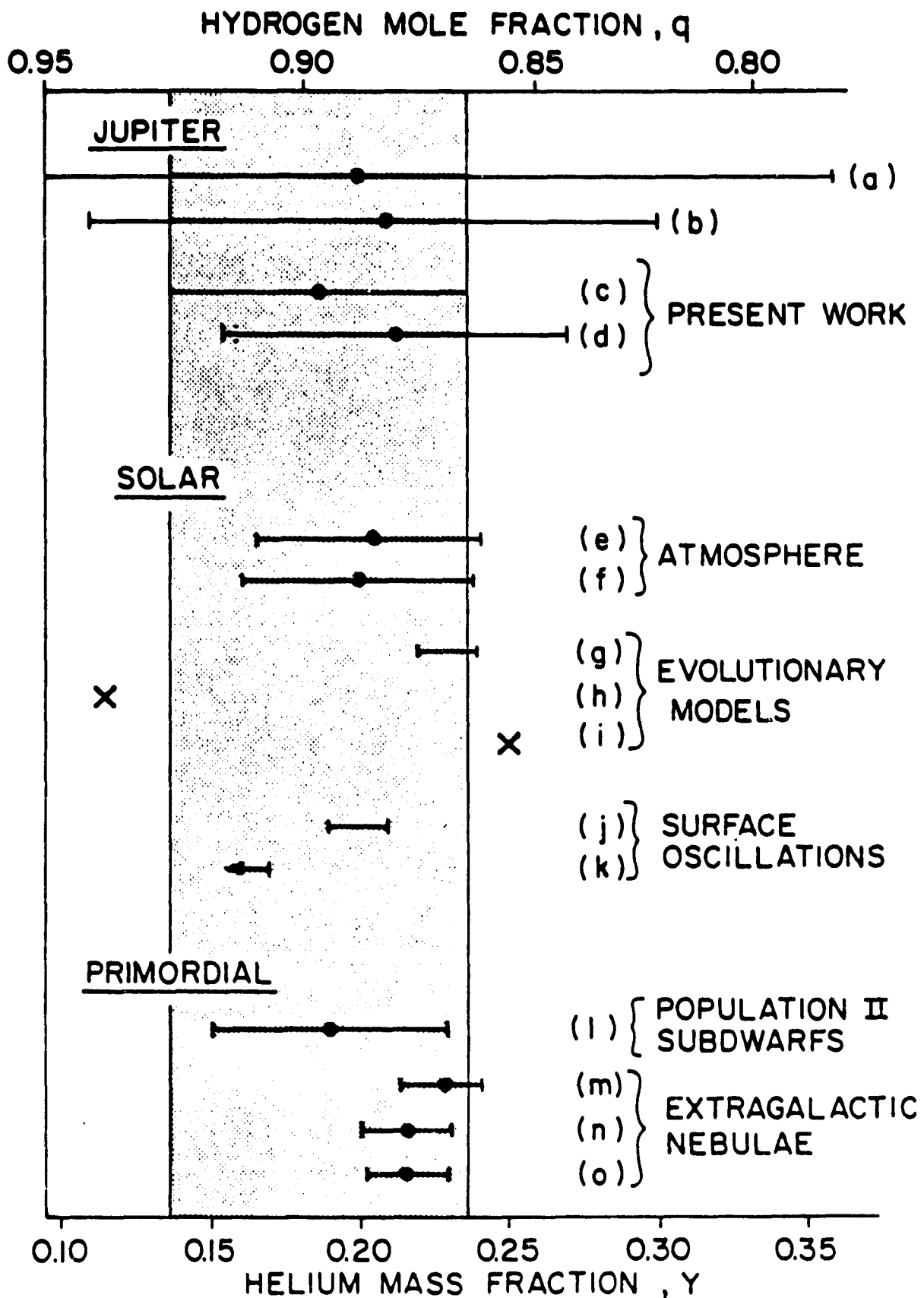


Figure 10